Atomic force microscopy imaging and related issues in signal processing: a preliminary work

Charles Soussen, David Brie, Fabien Gaboriaud, Cyril Kessler

ATOMIC FORCE MICROSCOPY IMAGING AND RELATED ISSUES IN SIGNAL PROCESSING: A PRELIMINARY WORK

Charles Soussen * **David Brie** * **Fabien Gaboriaud** ** **Cyril Kessler** *

* *Centre de Recherche en Automatique de Nancy (CRAN, UMR 7039, Nancy-University, CNRS), Boulevard des Aiguillettes, B.P. 239, F-54506 Vandœuvre-lès-Nancy, France*

** *Laboratoire de Chimie Physique et Microbiologie pour l'Environnement (LCPME, UMR 7564, Nancy-University, CNRS), 405, rue de Vandœuvre, 54600 Villers-lès-Nancy, France*

Abstract: Interatomic and intermolecular forces have been extensively studied, for their ability to understand the processes at the interface between solids and aqueous solutions. In particular, atomic force microscopy (AFM) generates tridimensional images and force profiles at nanometric scale, whatever the nature of the samples (biological, organic, mineral). An AFM microscope affords the measurement of interatomic forces exerting between a probe associated to a cantilever and a chemical sample. A force spectrum $f(z)$ shows the evolution of these forces as a function of the distance z between the probe and the sample. This is a pointwise analysis of the sample, obtained by measuring the cantilever deflection with respect to the probe-sample distance. A reproduction of this pointwise analysis, in conjunction with the scan of the sample surface yields a force-volume image $f(x, y, z)$. This image is composed of the collection of force spectra $f(z)$ on a grid (x, y) representing the sample surface. Today, the analysis and interpretation of a force-volume image remains mainly descriptive. In this paper, we introduce a signal processing formulation, which aims at a precise and automatic characterization of each pixel (x_i, y_i) of the sample surface. These problems include the decomposition of a force spectrum into elementary patterns, and the factorization of a force-volume image. We discuss the ability of standard signal processing methods to solve these problems, and we illustrate the discussion by means of experimental data.

Keywords: Nanotechnology, atomic force microscopy (AFM), force-volume imaging, tridimensional signals, convolutive mixture of signals, optimization of multidimensional criteria.

1. INTRODUCTION

Interatomic and intermolecular forces have been extensively studied, for their ability to understand the processes at the interface between solids and aqueous solutions. During the last decades, the development of near field microscopies has afforded to determine *in situ* local physico-chemical properties (electric, magnetic, vibration, forces) (Wiesendanger, 1994). In particular, atomic force microscopy (AFM) is capable to generate force profiles at nanometric scale, whatever the nature of the samples (biological, organic, mineral), and tridimensional (3D) images, called *force-volume images*.

Atomic force microscopy was invented in 1986 (Binnig, 1986) and the first prototype was exhibited a few months later (Binnig *et al.*, 1986). This discovery has motivated a great number of developments, at experimental and theoretical levels (Giessibl, 2003). Simultaneously, force spectroscopy appeared, with the ability to record force-volume images (Sokolov *et al.*, 1999; Heinz and Hoh, 1999; Butt *et al.*, 2005).

An AFM microscope is based on the measurement of interatomic forces exerting between a probe associated to a cantilever and a sample. A force spectrum $f(z)$ shows the evolution of these forces as a function of the distance z between the probe and the sample, as recorded from the piezo displacement. This is a pointwise analysis of the sample, obtained by measuring the cantilever deflection with respect to (w.r.t.) the probe-sample distance. A reproduction of this pointwise analysis, in conjunction with the scan of the sample surface yields a force-volume image $f(x, y, z)$. This image is composed of the collection of force spectra $f(z)$ on a grid (x, y) which represents the sample surface.

Today, the analysis and interpretation of a force-volume image remains mainly descriptive; to our knowledge, there is no signal processing method dedicated to force-volume imaging. Such tools would consist in:

(1) the 3D reconstruction of maps representing the topology of nano-objects, or the physico-chemical properties. The topologic reconstruction is a difficult problem which has not received, to our sense, a satisfactory solution. Its resolution will lead to major advances in the interpretation and exploitation of data generated by other techniques of near field microscopy (namely, optical techniques).

(2) the research of elementary physico-chemical components inside a force-volume image. When the sample to be analyzed is a mixture of heterogeneous components, the problem is to determine their number, to identify them, and to estimate their relative distribution in the mixture by source separation techniques. The development of multilinear factorization methods offers new perspectives, since they aim at decomposing multidimensional images by means of lower dimension descriptors (Harshman *et al.*, 2003). We can expect to retrieve elementary force interactions from force-volume images, and to provide their spatial distribution and their evolution as a function of physico-chemical conditions such as pH or ionic strength.

In the following section, we will describe the acquisition of spectroscopic data using the AFM instrument. We will emphasize the physical interactions occurring between the probe and the sample during a force profile acquisition, and give parametric models (Heinz and Hoh, 1999). In Sections 3, 4 and 5, we will introduce the analysis of force spectra and force-volume images in terms of signal processing problems, *e.g.,* the decomposition of a signal into elementary patterns and the factorization of a multidimensional image. We will illustrate these problems with a set of real data, corresponding to mineral colloidal particles whose chemical surface properties are heterogeneous and far to be understood.

2. AFM MICROSCOPY

The operating modes of an AFM microscope are based on the detection of interatomic forces (capillary, electrostatic, Van der Waals, friction) exerting between a cantilever-mounted probe and a sample surface. We generally distinguish two modes of data acquisition.

2.1 Contact and intermittent imaging modes

The probe performs the scanning of the whole sample surface, hence providing two-dimensional data. Two distinct modes are available:

- the contact (or static) mode. The probe and the sample remain in close contact during the raster scan. The contact mode directly provides the topology;
- the non contact mode. Typically, a variation of the interaction forces induces a variation of the resonant frequency of the cantilever, leading to a reduction of the oscillation amplitude. A closed-loop control system maintains the oscillation amplitude, as the feedback control signal is used to move the probe up and down, and keeps constant the force acting on the oscillation of the cantilever. Therefore, this mode yields isoforce images.

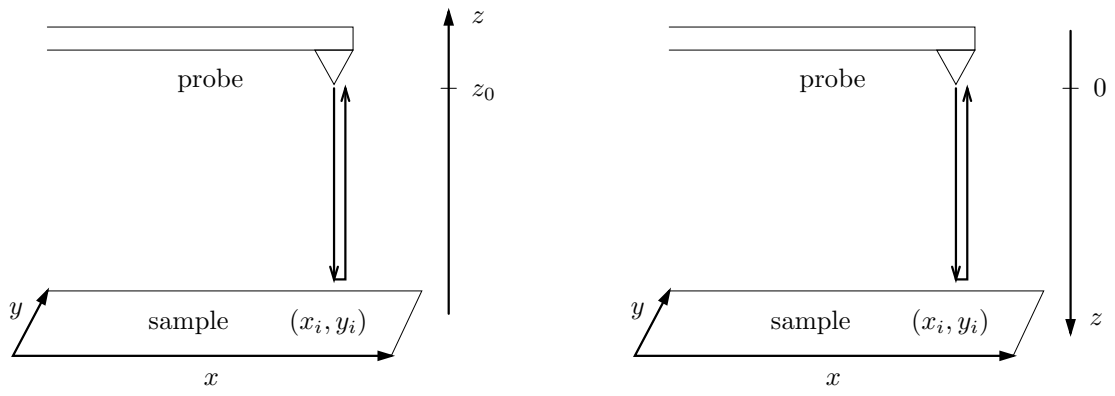

Fig. 1. Force spectroscopy. (a) At a pointwise location (x_i, y_i), the force measurements are collected while the probe approaches, and then retracts from the sample. (b) For convenience, we pre-process the data by reversing the orientation of the z axis, and we set $z = 0$ for the highest probe position.

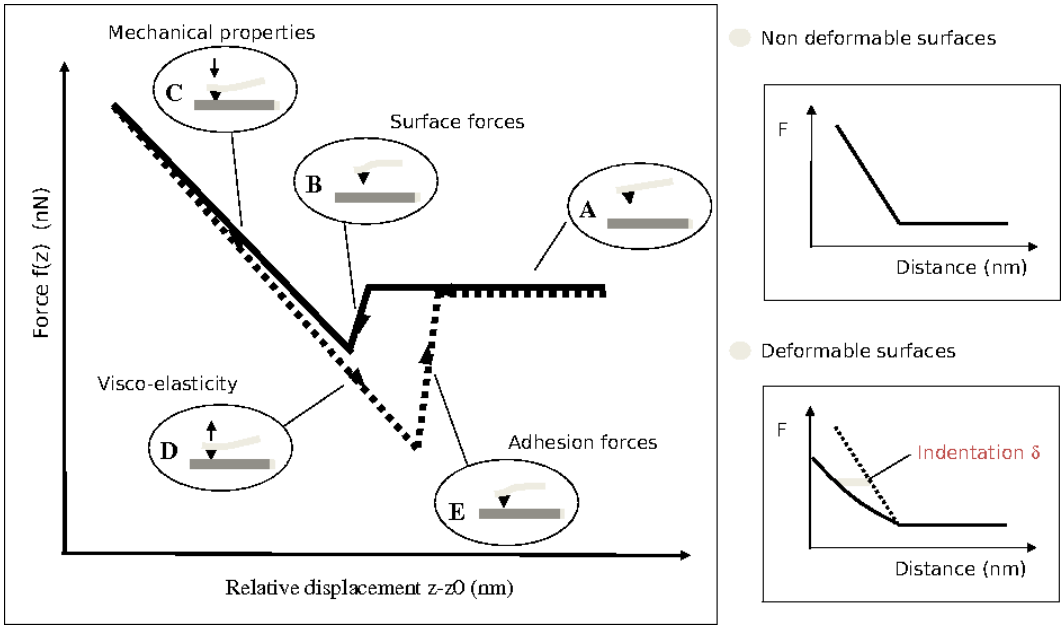

Fig. 2. General shape of a force spectrum. Approach (solid line) and retraction (dashed line) curves at a pointwise location (x_i, y_i). Adapted from (Gaboriaud and Dufrêne, 2007).

2.2 Force spectroscopy

Contrarily to the previous acquisition mode, force spectroscopy is a *pointwise* analysis of the sample, obtained by measuring the cantilever deflection as a function of the distance z between the probe and the sample surface (see figure 1). A force spectrum $f(z)$ shows the evolution of this force as a function of z at a specific location on the sample.

The general shape of a force spectrum is shown on figure 2. The force intensity is computed from relative measurements of the cantilever deflection, as a function of the relative motion of the probe $z - z_0$, where distance z_0 stands for the reference probe position, whose location is the most distant to the sample. A force profile is composed of two curves, corresponding to the approach and the retraction of the probe (in solid and dashed lines, respectively). In the following, we will describe the specific regions of interest on these curves.

2.2.1. Approach curve

- Region A: no interaction occurs when the cantilever is far from the sample. This region allows us to define the null value of the forces. Indeed, let us recall that the experimental force spectra are measured in a relative fashion, in terms of both probe motion and force values;
- Region B: surface forces (electrostatic, Van der Waals). These interactions are either negative (attraction between the probe and the surface), or positive (repulsion). Here, the probe is not in contact with the sample;

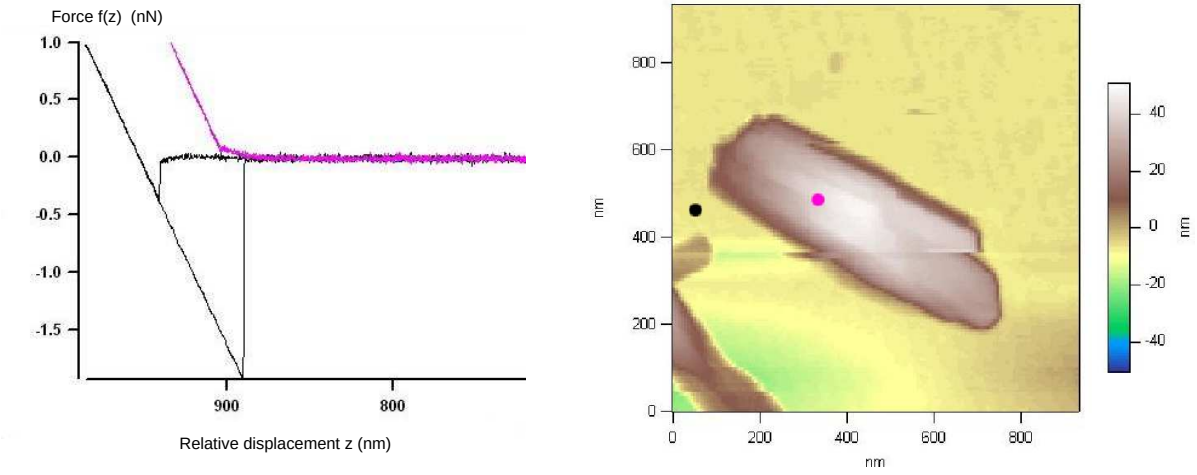

(a) (b)

Fig. 3. Application of the force-volume mode to a nanometric goethite particle (α-FeOOH) lain on a glass strip, in interaction with an AFM probe covered with an aluminum oxide of positive charge (pH = 4, $NaNO_3$ = 1 mM). (a) Recording of two force spectra, in the interior (repulsive interactions) and exterior (attractive interactions) of the goethite particle surface. (b) AFM image measured in the contact mode, in liquid environment.

- The contact between the probe and the sample is reached at the border between regions B and C;
- Region C describes the mechanical interactions of the cantilever and/or the sample. For a non deformable sample, this behavior is mainly due to the linear deformation of the cantilever. For a deformable sample, compression and/or indentation processes lead to linear or non linear behaviors.

2.2.2. Retraction curve

- Region D. During the retraction, the occurrence of an hysteresis between the approach and retraction curves is due to the viscoelastic properties of the sample. For non deformable surfaces, this hysteresis is equal to zero;
- Region E. Important adhesion forces may be embedded in the retraction curves, depending on the surface of contact, the contact duration, and mainly on the surface energy between the sample and the probe. For micro-organisms, this region is composed of numerous discontinuities.

2.3 Force-volume imaging

By reproducing the preceding pointwise analysis and by scanning the sample surface, we obtain a *force-volume* image $f(x, y, z)$ [1]. This image is formed of the collection of force spectra $f(z)$ on a grid (x, y) representing the sample surface (see figure 4 (a)).

The visualization of such 3D image is not obvious. A basic process considers each force spectrum separately, and then estimates the contact point between the probe and the sample. These estimations provide a 2D (incomplete) topologic reconstruction of the sample.

We now illustrate those notions, with a set of real data obtained in aqueous solutions using an MFP-3D instrument (Asylum Research, Santa Barbara, USA).

2.4 Experimental data

Figure 3 (a) displays the force spectra measured for a nanometric goethite particle (α-FeOOH) immobilized on a glass slide (Gaboriaud and Ehrhardt, 2003). The exhibited force profiles correspond to two pointwise locations on the sample surface. The first location belongs to the surface of the goethite particle while the second one is on the glass slide (see figure 3 (b)). Clearly, the topology is different in these two points, as the "contact points" between the probe and the sample (regions B-C of the spectra) are not reached for the same values of z. Moreover, the surface forces are alternatively repulsive and attractive for these two spectra.

[1] The signals and images measured in AFM microscopy are discrete, but we will rather, for simplicity reasons, use continuous notations for x, y, z, except when the discrete formalization will be necessary.

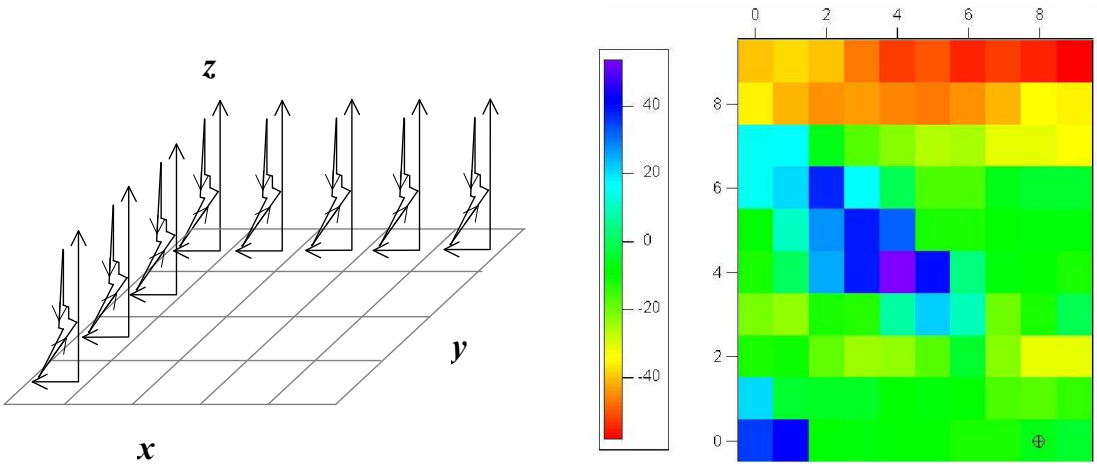

(a) (b)

Fig. 4. Force-volume imaging. (a) Recording of a force-volume image on a grid (x, y) representing the sample surface. (b) Imaging of a nano-particle of goethite. The displayed image is a 2D reconstruction representing the probe-sample contact for each point of the surface. This reconstruction is performed given a force-volume image recorded on a grid of 10×10 pixels.

The force-volume image data, which were measured during the AFM experiment, correspond to the scan of a surface $\{(x, y) \subset [X_{\min}, X_{\max}] \times [Y_{\min}, Y_{\max}]\}$ of size 1 μm^2. The sample surface was discretized into $100 = 10 \times 10$ square pixels (x_i, y_i), giving rise to the measurement of 100 force spectra $f(x_i, y_i, z)$. The 2D topologic reconstruction performed on this set of data, by analysis of the z displacement corresponding to the contact point, is displayed on figure 4 (b).

The data acquisition procedure has several specificities, which imply a data pre-processing step, for visualization and description purposes:

- the size of the force spectra depends on the local topology; a "deep" pixel (x_i, y_i) yields a large probe motion, and thus a large number of data values; in average, the 1D force spectra are composed of 2000 values;
- the force spectra are not uniformly sampled with respect to z, because of the numerical errors of the control of the probe motion during the approach and retraction phases;
- the recording of z values and force values are done in a relative fashion. Therefore, a pre-processing consists of searching for the zero value of each force spectrum, and reversing the orientation of the z values; see figure 1.

3. SIGNAL PROCESSING ISSUES

3.1 Visualization and extraction of information from AFM data

In Sections 4 and 5, we will introduce some signal processing issues, related to the handling of AFM data. Our goal is to develop automatic methods to characterize the sample surface given a force-volume image, as precisely as possible:

(1) firstly, extract partial information from this data volume, such as the sample topology;
(2) secondly, search for the elementary interaction forces in the data, in cases where the sample is a mixture of heterogeneous chemical components. The separation of these elementary components from the mixture (and the determination of their number), their identification, and the estimation of their relative weights in the mixture will be done by source separation techniques.

3.2 Assumptions and prerequisites

For convenience and clarity reasons, we will:

- reverse the orientation of the z axis, so that the low values of z (*i.e.,* large probe-sample distance) appear on the left of the z-axis, and conversely, large values of z (*e.g.,* contact between the probe and the sample) appear on the right of the spectrum (see figure 5). In particular, the zero value of z corresponds to the highest position of the probe, referred to as z_0 on figure 1 (a);
- only consider the approach curves in the case of the data displayed on figure 3. Straightforwardly, the mathematical formulations which will be presented shall be extended to the case of retraction curves.

In the following, we present two strategies to handle AFM data. The first works on 1D spectra independently (that is, $f(x_i, y_i, z)$ for fixed values of x_i and y_i), the second is a joint processing of all spectra $f(x, y, z)$.

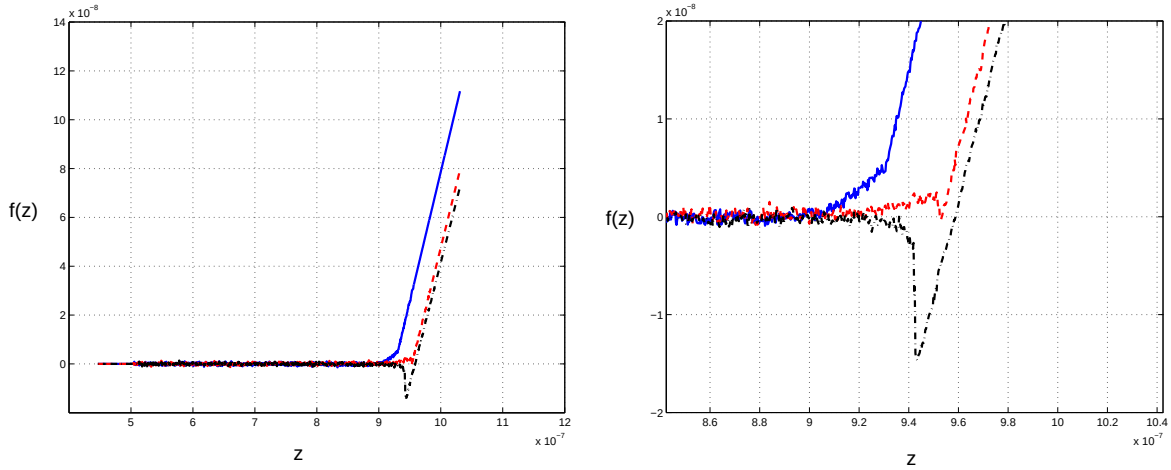

(a) (b)

Fig. 5. Three experimental force spectra (approach curve only) after the pre-processing step. (a) The solid and dashdot curves correspond to repulsive and attractive interactions, respectively. The dashed curve characterizes an heterogeneous interaction; this spectrum is composed of both repulsion and adhesion patterns. (b) Zoom in of (a).

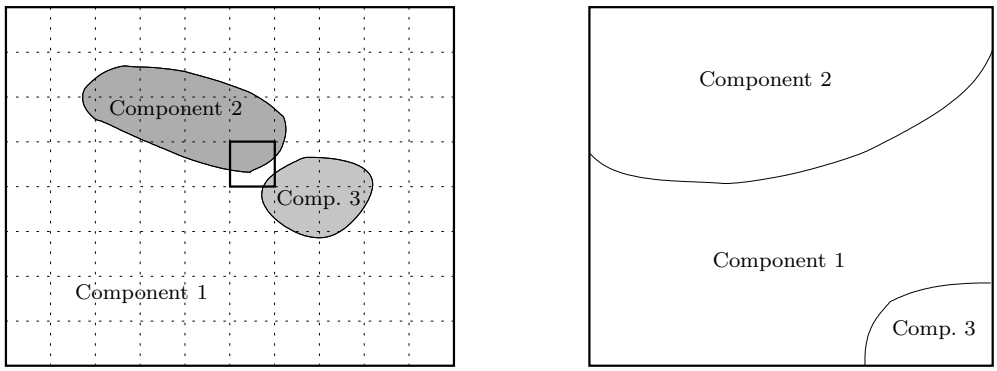

(a) Image grid (b) An heterogeneous pixel of grid (a)

Fig. 6. Discretization of the sample surface (x, y) into a set of square pixels. A pixel is referred to as homogeneous when its surface is composed of only one elementary component (*e.g.,* only component $k = 1$ occurs for the background pixels). (b) An heterogeneous pixel (x_i, y_i) is composed of a mixture of elementary components (here, components $k = 1$, 2 and 3). The goal of the force spectrum analysis is to retrieve the weight of the elementary components into each pixel (x_i, y_i).

4. ANALYSIS OF ONE SPECTRUM

This analysis aims at retrieving the regions A-E described above, from a given spectrum $f(z)$ (or regions A-C when processing an approach spectrum only). The precise estimation of characteristic parameters, such as the contact point (between regions B and C) describing the sample topology, or the location of discontinuities in the retraction curve, are crucial information for physicists.

In order to retrieve such patterns, it is essential to account for the physical models which describe the probe-sample interaction, in the approach (van der Waals, electrostatic, elastic forces) and retraction (adhesion and capillary forces, chemical bonding) phases. For each interaction, one can exhibit parametric models (Heinz and Hoh, 1999), which will be referred to as *parametric patterns*. We now distinguish homogeneous and heterogeneous interactions, depending whether the sample is a mixture of several elementary components or not at location (x, y) (see figures 5 and 6).

4.1 Homogeneous component

Let us consider a homogeneous component f_k (k-th component). One can express the interaction force by means of a parametric function.

For the data illustrated on figure 3, we distinguish two main components corresponding to:

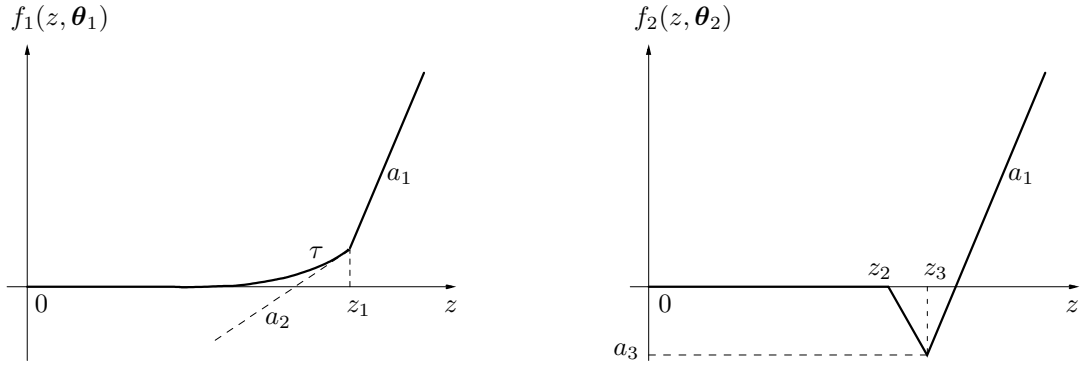

(a) (b)

Fig. 7. Repulsion (a) and adhesion (b) models for force spectra. The sets of parameters of both force spectra are $\boldsymbol{\theta}_1 = \{a_1, a_2, \tau, z_1\}$ and $\boldsymbol{\theta}_2 = \{a_1, z_2, z_3, a_3\}$, respectively.

(1) the nano-object ($k = 1$);
(2) the background ($k = 2$), *i.e.,* the glass slide on which the nano-object lies.

4.1.1. Repulsive interaction. The so-called interaction corresponds to the case of non deformable minerals (nano-objects), whose polarization are identical to that of the probe. The force spectrum is piecewise modeled by:

$$f_1(z, \boldsymbol{\theta}_1) = \begin{cases} a_2\tau \exp\left[(z - z_1)/\tau\right] & \text{if } z \leqslant z_1, \\ a_2\tau + a_1(z - z_1) & \text{if } z > z_1 \end{cases} \tag{1}$$

(see figure 7 (a)). The exponential and affine functions correspond to regions A & B and region C, respectively. Their first order derivatives at $z{=}z_1$ are equal to a_2 and a_1. The set of parameters is defined by $\boldsymbol{\theta}_1 = \{a_1, a_2, \tau, z_1\}$, where:

- z_1 is the z-value of the contact between the probe and the sample;
- τ is the shape coefficient of the exponential curve;
- a_1 is the slope of the affine function;
- a_2 is the left derivative of f_1 at $z = z_1$.

4.1.2. Adhesive interaction. The adhesion model is dedicated to non deformable materials, like the the glass slide corresponding to the background of figure 3 (a). As in the previous paragraph, we can express the force spectrum by use of a parametric model, which is here piecewise affine.

$$f_2(z, \boldsymbol{\theta}_2) = \begin{cases} 0 & \text{if } z \leqslant z_2, \\ a_3\,(z - z_2)/(z_3 - z_2) & \text{if } z_2 < z < z_3, \\ a_3 + a_1(z - z_3) & \text{if } z \geqslant z_3 \end{cases} \tag{2}$$

(see figure 7 (b)). The three affine functions correspond to regions A, B and C, respectively. The set of parameters is defined by $\boldsymbol{\theta}_2 = \{a_1, z_2, z_3, a_3\}$, where:

- z_2 refers to the transition between the regions A and B;
- z_3 is the z-value of the contact between the probe and the sample;
- a_3 is the force value $f(z_3)$;
- a_1 is the slope of the third affine function.

Remark. For both models (1) and (2), a_1 represents the slope of the last linear region. This parameter is an intrinsic characteristic of the AFM microscope.

4.2 Heterogeneous interaction

For an heterogeneous interaction, we express the force spectrum as the superposition of homogeneous component spectra. A visual inspection of the experimental spectra (see figure 5) leads to the following model:

$$f(z, \boldsymbol{\theta}) = f_1(z, \boldsymbol{\theta}_1) + f_2(z, \boldsymbol{\theta}_2), \tag{3}$$

where $\boldsymbol{\theta} = \{\boldsymbol{\theta}_1, \boldsymbol{\theta}_2\}$ is the set of parameters of the heterogeneous spectrum, that is $\boldsymbol{\theta} = \{z_1, z_2, z_3, \tau, a_1, a_2, a_3\}$. Note that the intrinsic parameter a_1 occurs in both f_1 and f_2, hence its value shall be set to half of the value of a_1 in (1) and (2).

Remark. An homogeneous component can be seen as a particular case of (3), where $z_3 = z_1$, and either a_3 or τ is equal to 0.

- When $\tau = 0$, we can continuously extend definition (1) by setting

$$f_1(z, \boldsymbol{\theta}_1) = \begin{cases} 0 & \text{if } z \leqslant z_1, \\ a_1(z - z_1) & \text{if } z > z_1. \end{cases} \tag{4}$$

  This spectrum is characteristic of the non-existing component ($k{=}1$). The spectrum $f_2(z, \boldsymbol{\theta}_2)$ corresponding to the existing component has the shape of figure 7 (b).
- When $a_3 = 0$, the homogeneous material is described by f_1. Equation (4) holds for $f_2(z, \boldsymbol{\theta}_2)$, where z_1 is now replaced by z_3.

In conclusion, the force spectrum of an homogeneous component can always be expressed as the sum of (4) and either (2) or (1), with $z_3 = z_1$.

In cases where the sample is heterogeneous, the estimation of the spectrum parameters $\boldsymbol{\theta} = \{\boldsymbol{\theta}_1, \boldsymbol{\theta}_2\}$ affords:

- the weight of both materials ($k = 1$ and $k = 2$) inside the current pixel (x, y), by means of $|a_3|$ and $a_2\tau$;
- the average topology of both materials inside the current pixel (z_1 and z_3).

4.3 Least squares approximation of the parametric model

We estimate the set of parameters $\boldsymbol{\theta}$ given the experimental data $\{(z_j, f_j), j = 1, \ldots, J\}$ by using the least squares method. The estimated parameter value is defined as the minimizer of the following cost function:

$$\mathcal{C}(\boldsymbol{\theta}) = \sum_{j=1}^{J} (f_j - f(z_j, \boldsymbol{\theta}))^2, \tag{5}$$

where function $f(z, \boldsymbol{\theta})$ is defined by (3), and J stands for the number of experimental data. More specifically, (5) can be replaced by:

$$\mathcal{C}_k(\boldsymbol{\theta}_k) = \sum_{j=1}^{J} (f_j - f_k(z_j, \boldsymbol{\theta}_k))^2, \tag{6}$$

when we know that the sample is locally homogeneous, and we have identified the corresponding model ($k = 1$ or 2).

The minimization of $\mathcal{C}$ is carried out under the following constraints:

$$\begin{cases} a_1 > 0, \\ \tau \geqslant 0, \\ a_3 \leqslant 0, \\ z_2 < z_3, \\ z_3 \leqslant z_1, \end{cases} \tag{7}$$

which account for the physical laws describing the probe-sample interaction. In particular, the last constraint states that the glass slide is always "deeper" than the sample which lies above it.

The constrained optimization of $\mathcal{C}$ is not an easy task. For instance, let us consider the minimization of $\mathcal{C}_2$ defined by (6) and (2), corresponding to an homogeneous sample of adhesive type. Clearly, $\mathcal{C}_2(\boldsymbol{\theta}_2)$ is a function of the four parameters $\boldsymbol{\theta}_2 = \{a_1, z_2, z_3, a_3\}$, and the dependence w.r.t. a_1 and a_3 is quadratic. Consequently, for fixed values of z_2 and z_3, we can directly compute the *exact* minimizer of $\mathcal{C}_2$ w.r.t. a_1 and a_3:

$$\widehat{\mathcal{C}}_2(z_2, z_3) = \min_{a_1, a_3} \mathcal{C}_2(a_1, z_2, z_3, a_3), \tag{8}$$

at an inexpensive cost.

An interesting strategy is then to minimize $\widehat{\mathcal{C}}_2$ instead of $\mathcal{C}_2$, under the only constraint $z_2 < z_3$. On figure 8, we display an experimental AFM spectrum $\{(z_j, f_j), j = 1, \ldots, J\}$ and the related criterion $\widehat{\mathcal{C}}_2(z_2, z_3)$, computed on a grid (z_2, z_3) of $\mathbb{R}^2$. Figure 8 shows that there are two local minimizers, which we denote:

- (z_2^g, z_3^g): the local minimizer which is also the global minimizer of $\widehat{\mathcal{C}}_2$;
- (z_2^l, z_3^l): the other local minimizer, giving a larger value of the cost function.

The multimodality of $\mathcal{C}_2$ implies that local descent algorithms do not necessarily provide (z_2^g, z_3^g). Actually, this solution is very unlikely to be reached due to the very narrow shape of the basin of attraction of (z_2^g, z_3^g), unless the initial solution belongs to this basin. Moreover, the basin of attraction of (z_2^l, z_3^l) is of flat shape, leading to additional numerical difficulties: local descent algorithms may not even reach (z_2^l, z_3^l).

When minimizing criterion $\mathcal{C}_1(\boldsymbol{\theta}_1)$ by a similar approach, we encountered the same difficulties (multimodality of $\widehat{\mathcal{C}}_1$, flat basins of attraction). Classical local descent algorithms may fail to reach the global and the local minimizers of $\widehat{\mathcal{C}}_1$, and are sensitive to the initial value of the parameters. Numerical instabilities are also due to the exponential function involved in (1); for a fixed value of z ($z < z_1$), $f_1(z, \boldsymbol{\theta}_1)$ is very sensitive to variations of τ when τ is larger to some threshold value, and almost not when $\tau \approx 0$.

4.4 Topologic reconstruction from a force-volume image

The full visualization of a force-volume image $f(x, y, z)$ is not an obvious task. One generally performs the two following steps:

(1) For each 1D spectrum (location (x, y) is fixed), estimate the corresponding set of parameters $\boldsymbol{\theta}(x, y)$;
(2) Once the characteristic patterns of each spectrum are retrieved, display a few 2D images representing the sample topology (parameters z_1 and/or z_3), the energy of adhesion (*i.e.,* the surface of the region located under the exponential curve for repulsive interaction), *etc.*

We refer the reader to figure 4 (b) for a 2D topologic reconstruction result related to the experimental data.

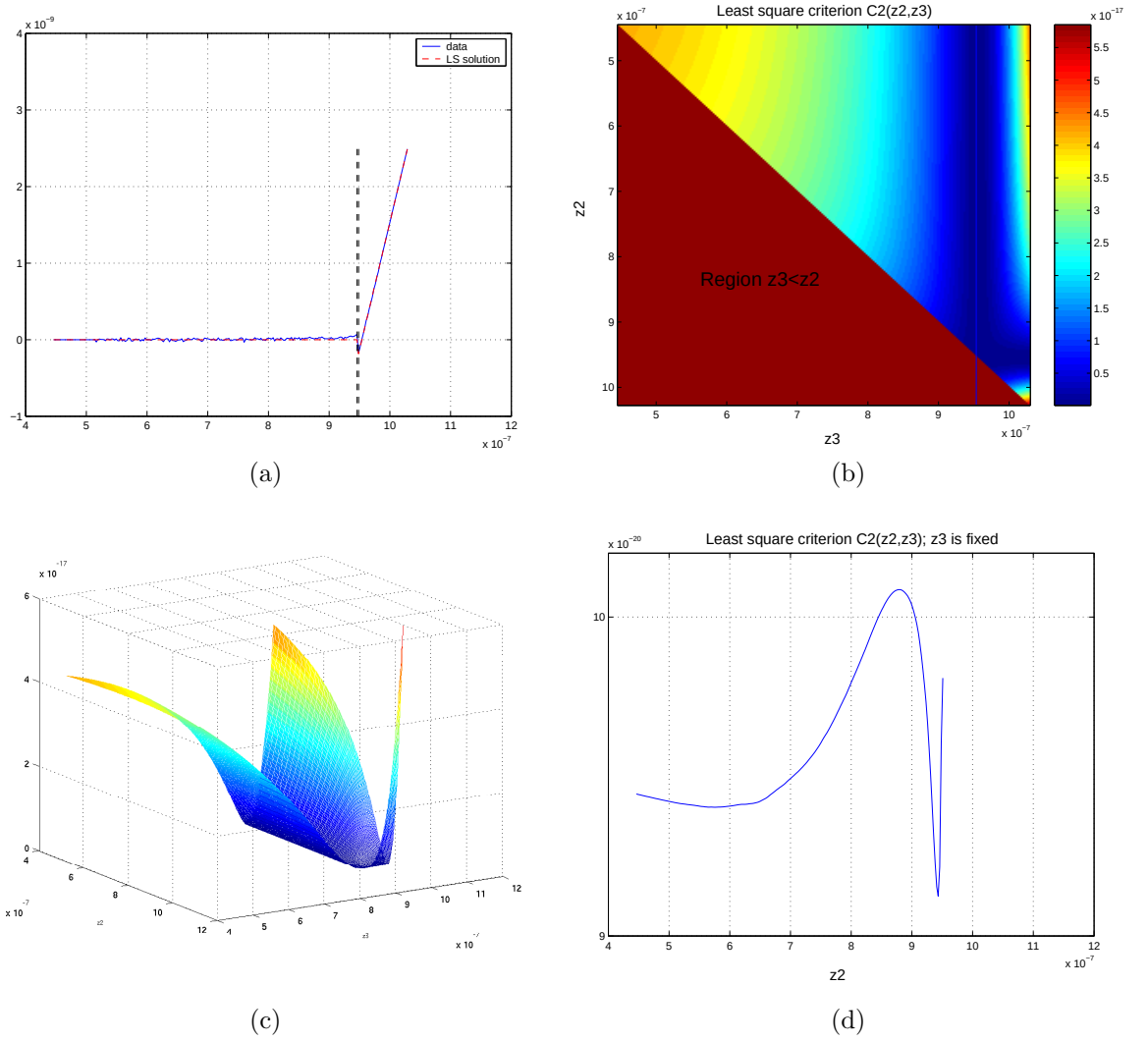

(a) (b) (c) (d)

Fig. 8. Least square approximation of the adhesion model $f_2(z, \boldsymbol{\theta}_2)$ to an experimental data spectrum. (a) The 1D experimental data (z_j, f_j) are displayed together with the parametric spectrum $f_2(z, \boldsymbol{\theta}_2)$ giving the lowest least-square error. The two vertical dashed lines refer to the locations (z_2, z_3) for which $\widehat{\mathcal{C}}_2(z_2, z_3)$ is minimal. Here, z_2 and z_3 correspond to two consecutive z-value z_j and z_{j+1}, hence yielding very close vertical lines. (b,c) 2D and 3D representations of criterion $\widehat{\mathcal{C}}_2(z_2, z_3)$, as defined in (8). The criterion is displayed on the domain $\{\min\{z_j\} \leqslant z_2 < z_3 \leqslant \max\{z_j\}\}$. (d) One dimensional profile of $\widehat{\mathcal{C}}_2(z_2, z_3)$, obtained for a fixed value of z_3 (profile along the vertical line of figure (b). This profile illustrates the multimodality of $\widehat{\mathcal{C}}_2$.

5. JOINT ANALYSIS OF A SET OF SPECTRA

The separate analysis of a single force spectrum is difficult to carry out, as the related optimization problem, described above, often leads to either local minima, either numerical difficulties. Although the use of global minimization procedures or specific dynamic programming algorithms can bring an improvement over local methods, we believe that the joint analysis of all the 1D spectra, in other words the force-volume image $f(x, y, z)$, will afford us to retrieve more details, since a force-volume image accounts for the spatial structure of the sample.

5.1 Convolutive mixture model

The force-volume image analysis aims at characterizing each pixel (x_i, y_i) of the sample surface given the entire 3D data $f(x, y, z)$. Let us consider an heterogeneous sample, composed of p elementary homogeneous components (called *sources*). We will assume that each data spectrum $f(x_i, y_i, z)$ (i-th pixel) is the result of a combination of the source spectra, denoted by $f_1(z), f_2(z), \ldots, f_p(z)$. To obtain this description, we use a model of convolutive mixture of sources, which accounts for the sample variation of topology along x and y:

$$f(x_i, y_i, z) = \sum_{k=1}^{p} a_{ik}\, f_k(z - z_{ik}), \qquad (9)$$

where:

- coefficient a_{ik} is the contribution of the k-th source at the interior of the i-th pixel;
- functions f_k are identical to the functions f_1 and f_2 defined in the particular case of repulsive and adhesive interactions with a non deformable sample. Other types of interactions may also occur, namely in the case of deformable nano-objects and in the retract phase;
- distances z_{ik} are homogeneous to probe-sample distances, and characterize the topology of the k-th source at the interior of the i-th pixel. These parameters are identical to z_1 and z_3 in (1) and (2).

Clearly, the occurrence of several sources in the interior of the same pixel indicates that the chemical sample is locally heterogeneous ($a_{ik} \neq 0$ for the i-th pixel and for several values of k); see figure 6.

The joint estimation of the sources, their topology and the mixture coefficients from a force-volume image $f(x, y, z)$ can be seen as a source separation problem. It is a classical signal processing problem, which however, is far to be trivial for convolutive mixtures.

5.2 Source separation from convolutive mixtures

Equation (9) rereads:

$$f(x_i, y_i, z) = \sum_{k=1}^{p} a_{ik} \left(\delta_{z_{ik}} \underset{z}{*} f_k\right)(z), \qquad (10)$$

where $\delta_{z_{ik}}(z) = \delta(z - z_{ik})$ represents the 1D Dirac distribution. Clearly, (10) reduces to the classical instantaneous linear model encountered in source separation, when the parameters z_{ik} are all equal to zero, *i.e.,* when sample topology is flat. When the topology is not flat, the source separation problem is specially difficult, since the sample topology is unknown, as well as the sources and their respective weights in the mixture. In a formal viewpoint, model (10) is non linear w.r.t. parameters z_{ik}. However, the 1D Fourier transform of $f(x_i, y_i, z)$ w.r.t. z reads:

$$\widetilde{f}(x_i, y_i, \nu_z) = \sum_{k=1}^{p} a_{ik} \exp\left(-2j\pi\nu_z z_{ik}\right) \widetilde{f}_k(\nu_z), \qquad (11)$$

denoting by "$\widetilde{\cdot}$" the 1D Fourier transform operator, and by ν_z the frequencies along z. This model is now bilinear w.r.t. a_{ik}, $\exp\left(-2j\pi\nu_z z_{ik}\right)$, and signals $\widetilde{f}_k(\nu_z)$.

5.3 Inversion of the convolutive mixture model

The inversion of the mixture model amounts to estimating the mixture parameters, *i.e.,* coefficients a_{ik}, z_{ik}, and the source signals f_k (and their number p) given the experimental data and model (10). It is well known that the source separation problem is an ill-conditioned inverse problem, which suffers from several indeterminacies. In particular, we have:

$$\delta_{z_{ik}} * f_k = \left(\delta_{z_{ik}} * \delta_{-z'_k}\right) * \left(\delta_{z'_k} * f_k\right). \qquad (12)$$

In other words, the sources f_k can only be separated up to a delay z'_k.

As seen in section 4, the physical models describing the interactions which occur during the motion of the probe (approach or retraction) are available. They provide us with parametric models of the source signals f_k, also referred to as decomposition into elementary patterns:

$$f_k(z) = f_k(z, \boldsymbol{\theta}_k), \qquad (13)$$

where the so-called patterns (discontinuity, exponential curve, *etc.*) embedded into the elementary spectra are described by the set of parameters $\boldsymbol{\theta}_k$.

We expect that the use of multilinear tensor factorization algorithms (Harshman *et al.*, 2003), coupled with this parametric decomposition of sources, will afford us to solve the problem of source separation from convolutive mixtures.

5.4 Accounting for the probe geometry

The model (10) describing the probe-sample force interactions is often unrealistic, since it does not account for the probe geometry. The latter model is only valid when the width of the probe is negligible w.r.t. the size of the square pixels (x_i, y_i) discretizing the sample surface.

When this condition is not satisfied, one needs a more realistic model, which also involves a convolution in the (x, y) domain (Udpa *et al.*, 2006). Let us assume that the probe is of non deformable parallelepipedic shape (see figure 9). This assumption amounts to considering that a pixel (x_i, y_i) of the sample surface is submitted to a force distribution related to the probe geometry.

For an homogeneous sample (component k only), (10) rereads:

$$f(x, y, z) = f_k(z - z_{xyk}), \qquad (14)$$

where x_i, y_i, and the topologic parameters z_{ik} are replaced by continuous notations, and the weight factor a_{xyk} is omitted. The extension of (14) to the case of a finite width probe reads:

$$f(x, y, z) = h(x, y) \underset{(x,y)}{*} f_k(z - z_{xyk}), \qquad (15)$$

where the point spread function h is defined by:

$$h(x, y) = \begin{cases} 1 \text{ if } (x, y) \in [x_{\min}, x_{\max}] \times [y_{\min}, y_{\max}], \\ 0 \text{ otherwise,} \end{cases} \qquad (16)$$

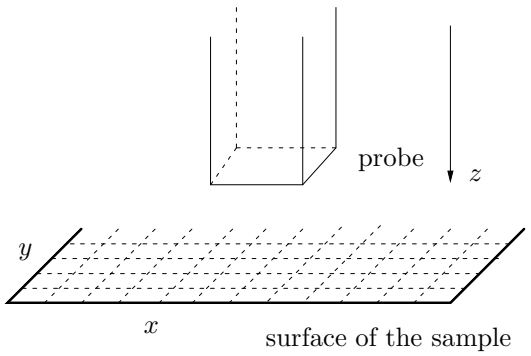

Fig. 9. Accounting for the probe geometry. Here, the shape of the probe is modeled as a non deformable parallelepipedic material.

and $\big[x_{\min}, x_{\max}\big] \times \big[y_{\min}, y_{\max}\big]$ stands for the horizontal cross-section of the probe.

For an heterogeneous sample, we generalize the above model as follows:

$$f(x,y,z) = h(x,y) \underset{(x,y)}{*} \sum_{k=1}^{p} \Big[a_{xyk}\, f_k(z - z_{xyk}) \Big]. \tag{17}$$

When the force-volume image data are finely resoluted along the (x,y) dimension, we can expect to reconstruct p fine resoluted images representing the sample topology z_{xyk} $(k = 1,\ldots,p)$ and p maps representing the weights a_{xyk} of the elementary components $(k = 1,\ldots,p)$. The joint estimation of h and of the mixture parameters can then be expressed as a deconvolution problem, coupled with a source separation problem. A natural strategy to cope with it is to process the following three steps:

(1) identify the point spread function $h(x,y)$. This step can be done by means of a learning sequence, corresponding to a mineral flat nano-object lying on a glass slide;
(2) solve the deconvolution problem, and thus remove the effect of $h(x,y)$;
(3) finally, solve the source separation problem (10), in which the probe is of negligible width.

Note that models (15) and (17) may be generalized when the probe extremity is not of flat shape. The point spread function h would not only depend on (x,y), but also on z to account for the relative depth of the probe extremity.

6. CONCLUSIONS

In this paper, we have briefly introduced the AFM modalities, and the physical processes which are related to the record of force spectra and force-volume images. Firstly, we have exhibited some parametric models describing an homogeneous component alone by a collection of shape factors (discontinuities of the spectrum, spatial topology of the component). Secondly, we have introduced a convolutive mixture model describing heterogeneous interactions, where the mixture model refers to the homogeneous components embedded in a given pixel, and the convolution operator accounts for the topology of the elementary components inside a pixel, and for the probe geometry. We have illustrated these models with a set of experimental data obtained in aqueous solutions using an MFP-3D instrument.

From a signal processing standpoint, future works will aim at developing advanced methods dedicated to force-volume images, namely the decomposition of a 1D spectrum into elementary patterns, the factorization and the deconvolution of a force-volume image. We believe that the simultaneous process of all 1D spectra, *i.e.,* of a force-volume image, will bring more accurate results than the separate analysis of each 1D force spectrum. We expect that the use of multilinear tensor factorization algorithms, coupled with the parametric description of elementary spectra, will afford us to solve the problem of source separation from convolutive mixtures.

ACKNOWLEDGMENT

The authors would like to thank Pr. Jérôme Idier for his helpful comments on the optimization part.

REFERENCES

Binnig, G. (1986). Atomic force microscope and method for imaging surfaces with atomic resolution. *US Patent* **4**(724), 318.

Binnig, G., C. F. Quate and C. Gerber (1986). Atomic force microscope. *Physical Review Letters* **56**(9), 930–933.

Butt, H.-J., B. Cappella and M. Kappl (2005). Force measurements with the atomic force microscope: technique, interpretation and applications. *Surface Science Reports* **59**(1–6), 1–152.

Gaboriaud, F. and J.-J. Ehrhardt (2003). Effects of different crystal faces on surface charge of colloidal goethite (a-FeOOH) particles: an experimental and modeling study. *Geochimica and Cosmochimica Acta* **67**(5), 967–983.

Gaboriaud, F. and Y. F. Dufrêne (2007). Atomic force microscopy of microbial cells: application to nanomechanical properties, surface forces and molecular recognition forces. *Colloids and Surfaces B: Biointerfaces* **54**, 10–19.

Giessibl, F. J. (2003). Advances in atomic force microscopy. *Review of Modern Physics* **75**(3), 949–983.

Harshman, R. A., S. Hong and M. E. Lundy (2003). Shifted factor analysis – Part I: Models and properties. *J. Chemometrics* **17**(7), 363–378.

Heinz, W. F. and J. H. Hoh (1999). Spatially resolved force spectroscopy of biological surfaces using atomic force microscope. *Trends in Biotechnology* **17**(4), 143–150.

Sokolov, I. Y., G. S. Henderson and F. J. Wicks (1999). Force spectroscopy in non-contact mode. *Applied Surface Science* **140**(3–4), 358–361.

Udpa, L., V. M. Ayres, Y. Fan, Q. Chen and S. A. Kumar (2006). Deconvolution of atomic force microscopy data for cellular and molecular imaging. *IEEE Signal Processing Magazine* **23**(3), 73–83.

Wiesendanger, R. (1994). *Scanning Probe Microscopy and Spectroscopy: Methods and Applications*. Cambridge Univ. Press, Cambridge, MA.